

A late-Ediacaran crown-group sponge animal

<https://doi.org/10.1038/s41586-024-07520-y>

Received: 29 July 2023

Accepted: 3 May 2024

Published online: 5 June 2024

 Check for updates

Xiaopeng Wang^{1,2,3}, Alexander G. Liu³, Zhe Chen^{1,2}, Chengxi Wu^{1,2}, Yarong Liu^{1,2}, Bin Wan^{1,2,✉}, Ke Pang^{1,2}, Chuanming Zhou^{1,4}, Xunlai Yuan^{1,2,✉} & Shuhai Xiao^{5,✉}

Sponges are the most basal metazoan phylum¹ and may have played important roles in modulating the redox architecture of Neoproterozoic oceans². Although molecular clocks predict that sponges diverged in the Neoproterozoic era^{3,4}, their fossils have not been unequivocally demonstrated before the Cambrian period^{5–8}, possibly because Precambrian sponges were aspiculate and non-biomineralized⁹. Here we describe a late-Ediacaran fossil, *Helicolocellus cantori* gen. et sp. nov., from the Dengying Formation (around 551–539 million years ago) of South China. This fossil is reconstructed as a large, stemmed benthic organism with a goblet-shaped body more than 0.4 m in height, with a body wall consisting of at least three orders of nested grids defined by quadrate fields, resembling a Cantor dust fractal pattern. The resulting lattice is interpreted as an organic skeleton comprising orthogonally arranged cruciform elements, architecturally similar to some hexactinellid sponges, although the latter are built with biomimetic spicules. A Bayesian phylogenetic analysis resolves *H. cantori* as a crown-group sponge related to the Hexactinellida. *H. cantori* confirms that sponges diverged and existed in the Precambrian as non-biomimeticizing animals with an organic skeleton. Considering that siliceous biomimeticization may have evolved independently among sponge classes^{10–13}, we question the validity of biomimeticized spicules as a necessary criterion for the identification of Precambrian sponge fossils.

Morphologically diverse animal fossils have been recognized in fossil assemblages of the late-Ediacaran period (around 575–539 million years ago (Ma)) and include examples of total-group eumetazoans¹⁴, cnidarians^{15,16} and bilaterians¹⁷. These fossils, along with molecular clock estimates^{2,3} and contentious biomarker data^{18–20}, demand an Ediacaran existence of sponges, which are probably the most basal animal phylum¹. However, few sponge fossils have been found from the Ediacaran period or earlier^{5,7,21}. The absence of Precambrian sponge fossils has been attributed to the low preservation potential of siliceous sponge spicules due to low Al³⁺ concentrations in Precambrian porewaters²² or to the possibility that early sponges were aspiculate and entirely non-biomimeticizing animals⁹. Here we report a crown-group sponge fossil, *Helicolocellus cantori* gen. et sp. nov., from the late-Ediacaran Shibantan limestone in South China (Extended Data Fig. 1). This new fossil is characterized by an organic latticework skeleton that is compositionally different from, but architecturally similar to and probably related to, spiculate hexactinellid sponges. It thus fills the late Neoproterozoic gap in sponge evolution and indicates that Precambrian sponges may have been aspiculate and non-biomimeticizing animals, particularly if biomimeticized skeletons evolved independently among sponge classes^{10–13}.

Systematic palaeontology

Phylum Porifera Grant, 1836

Helicolocellus cantori gen. et sp. nov.

Etymology. Genus name from Greek/Latin *helix*, helix; and Latin *locellus*, small box. Species epithet in honour of the mathematician Georg Cantor (1845–1918), with reference to the Cantor set, which describes the regular, self-similar pattern of subdivided rectangular lattices as observed in this fossil.

Holotype. NIGP-176531 (Figs. 1 and 2) part and counterpart, deposited in the Nanjing Institute of Geology and Palaeontology (NIGP).

Referred material. Paratype: NIGP-176532. Other specimens: NIGP-176533–176538 (Fig. 3 and Extended Data Fig. 2).

Locality and horizon. From the upper-Ediacaran Shibantan Member of the Dengying Formation at Wuhe, Yangtze Gorges area, Hubei Province, South China.

Diagnosis. A conical to subcylindrical body connected by means of a stem to a basal discoidal structure. The outer surface of the conical body is characterized by regularly arranged rectangles each subdivided into at least three orders of smaller rectangles, forming a hierarchical quadrate reticulation. Rectangles are orthogonally arranged in the upper portion of specimens and become helically twisted around the longitudinal axis towards the base. Rectangles are outlined by grooves which represent an organic cruciform skeletal structure.

Description. The holotype is preserved in positive relief on a bed top (Fig. 1), with a fragmentary impression of the corresponding negative relief preserved on a bed sole (Fig. 2b–d). *H. cantori* gen. et sp. nov. has a goblet-like morphology with a holdfast, a stem and a conical body, indicating a probable erect benthic lifestyle. The conical body is 291 mm in length (or height in reconstructed life orientation), with a maximum width of 108 mm, tapering basally to a connection

¹State Key Laboratory of Palaeobiology and Stratigraphy, Nanjing Institute of Geology and Palaeontology, Chinese Academy of Sciences, Nanjing, China. ²University of Chinese Academy of Sciences, Beijing, China. ³Department of Earth Sciences, University of Cambridge, Cambridge, UK. ⁴University of Chinese Academy of Sciences, Nanjing, Nanjing, China. ⁵Department of Geosciences and Global Change Centre, Virginia Tech, Blacksburg, VA, USA. [✉]e-mail: binwan@nigpas.ac.cn; xlyuan@nigpas.ac.cn; xiao@vt.edu

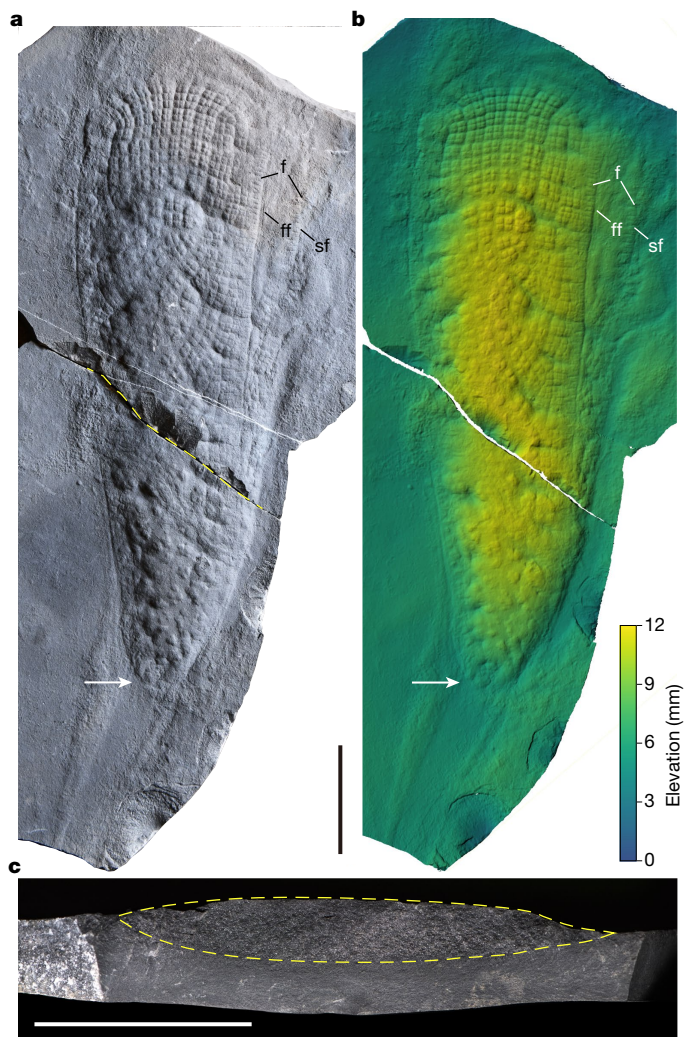


Fig. 1 | Holotype of *H. cantorigen. et sp. nov.*, NIGP-176531. **a,b.** Positive relief on bed top: photographed under reflected light directed from the upper right (**a**) and topographic elevation map from laser scanning microscopy (**b**). White arrows mark transition from bottom of conical body to the stem. The specimen is broken into two pieces along the yellow dashed line in **a**. **c.** Fracture surface along the breakage in **a** exposes a cross-section through the holotype specimen, showing a three-dimensional outline (dashed ellipse) infilled with coarser sparry calcite cement, in contrast to fine-grained micritic matrix. **f**, fringe; **ff**, first fringe; **sf**, second fringe. Scale bars, 50 mm.

with the stem. The stem is partially preserved as a flat and smooth impression, with a width of 23 mm, but the basal disc of the holotype is not preserved. The positive-relief specimen is broken into two parts (along the yellow dashed line in Fig. 1a and perpendicular to the bedding plane), allowing the observation of an elliptical cross-section through the partially flattened body, which is infilled with sparry calcite cement (Fig. 1c), implying an originally conical body with a central cavity.

The body wall exhibits a hierarchical latticework of rectangles, each of which bulges outwardly with a convex surface on the top bedding surface (Fig. 1b). The largest (first-order) rectangles (Fig. 2a,b) are subdivided into smaller rectangles, here termed second- and third-order rectangles (Fig. 2b–e). There are eight first-order rectangles per half-circumference along the distal end of the body. First-order rectangles are 12 ± 1.8 (1σ) mm long and 8.9 ± 1.2 (1σ) mm wide on average ($n = 41$ rectangles). They are separated from each other by grooves which are 1.1 mm wide and approximately 0.4 mm deep. Finer grooves

(0.61 mm wide and about 0.2 mm deep) subdivide the first-order rectangles into four equal second-order rectangles, which have an average length and width of 5.3 ± 0.9 (1σ) mm and 3.8 ± 0.7 (1σ) mm, respectively ($n = 164$ rectangles). The second-order rectangles are further subdivided into third-order rectangles, which are 2.55 mm long and 1.8 mm wide ($n = 146$ rectangles), by successively finer grooves (0.3 mm wide and about 0.1 mm deep). Fourth-order rectangles are faintly preserved (Fig. 2d,e).

In the distal region, rectangles are oriented in transverse rows parallel to the arched top edge of the body. Rectangles become diagonally aligned in the middle part of the body. The basal part of the conical body is often poorly preserved, consisting of vaguely defined but poorly aligned rectangles without fine structure, possibly resulting from postmortem distortion, as evidenced by a separate specimen showing regularly and diagonally arranged rectangles at the basal part (Extended Data Fig. 2d). The holotype exhibits two fringes on one side of the body (the right-hand margin in Fig. 1a,b). The fringes each consist of a single row of rectangles, although one of them (labelled 'ff' in Fig. 1a,b; hereafter, first fringe) has more sharply defined rectangles than the other (labelled 'sf' in Fig. 1a,b; hereafter, second fringe). It is possible that the first fringe represents a longitudinal furrow or suture in the body wall. Alternatively, the two fringes may be attributed to the conical body splitting along a single seam due to compaction. The alignment of neighbouring rectangles in the main body seems to be congruent with those that comprise the fringes (Figs. 1a,b and 2a).

In addition to the holotype, seven other specimens are known (Fig. 3 and Extended Data Fig. 2), two of which are complete (Fig. 3a,c). The paratype NIGP-176532 (Fig. 3a) is 447 mm long and up to 93 mm wide. It possesses a basal disc (Fig. 3a; 57 mm in diameter), which is connected to the conical body (284 mm long) by means of a stem (163 mm long, 30 mm wide). The stem is smooth, with two broader regions where its width expands from 32 mm to 48 mm (arrows in Fig. 3a). The basal disc and stem are both preserved in positive relief on the bed top, whereas the conical body is a negative relief impression. The first-order rectangles have an average length of 12.2 mm ($\sigma = 1.7$) and a width of 9 mm ($\sigma = 1.8$) ($n = 15$ measurements). They are subdivided into second-order rectangles, which are approximately 5.2 mm long and 4 mm wide. The second complete specimen, NIGP-176536 (Fig. 3c), is only 113 mm long. It comprises a conical body that is 65 mm long and 38 mm wide, and a stem that is 48 mm long and 11 mm wide. It has a truncated distal end possibly representing an artefact of breakage. A basal disc is not present. The poorly defined and irregularly arranged first-order rectangles are about 7.3 mm long and 6.6 mm wide. The irregular arrangement of rectangles is also observed in specimens NIGP-176536 (Fig. 3b) and NIGP-176534 (Extended Data Fig. 2a). By contrast, specimen NIGP-176538 exhibits well-preserved, diagonally arranged rectangles in the lower part of the conical body (Extended Data Fig. 2d). One of the incomplete specimens, NIGP-176535, shows a single marginal fringe (Extended Data Fig. 2c) rather than double fringes as observed in the holotype.

The preservation style of *Helicolocellus* is identical to that of other non-biomineralized macrofossils in the Shibantan Member, including *Arborea*²³, *Flabellophyton*²⁴ and *Wutubus*²⁵. Specifically, the distinction between the fossils and the sedimentary matrix is defined by lithological contrast, with proportionally more carbonate cement in the sediment filling the central cavity of the conical body (compare Fig. 1c with Fig. 7.2 of ref. 23, Fig. 9E of ref. 24 and Fig. 6g,h of ref. 25). The fossils are preserved as casts and moulds, but the body walls and their constituent elements are not preserved. This taphonomic style differs markedly from that of biomineralized tubular fossils such as *Cloudina*²⁶ and *Sinotubulites*²⁷ from the Shibantan Member, which preserve well-defined although secondarily replaced tests. This difference is probably because organic walls are more easily degraded and partially compacted (Fig. 1c), whereas a biomineralized test would be expected to retain its original three-dimensional morphology.

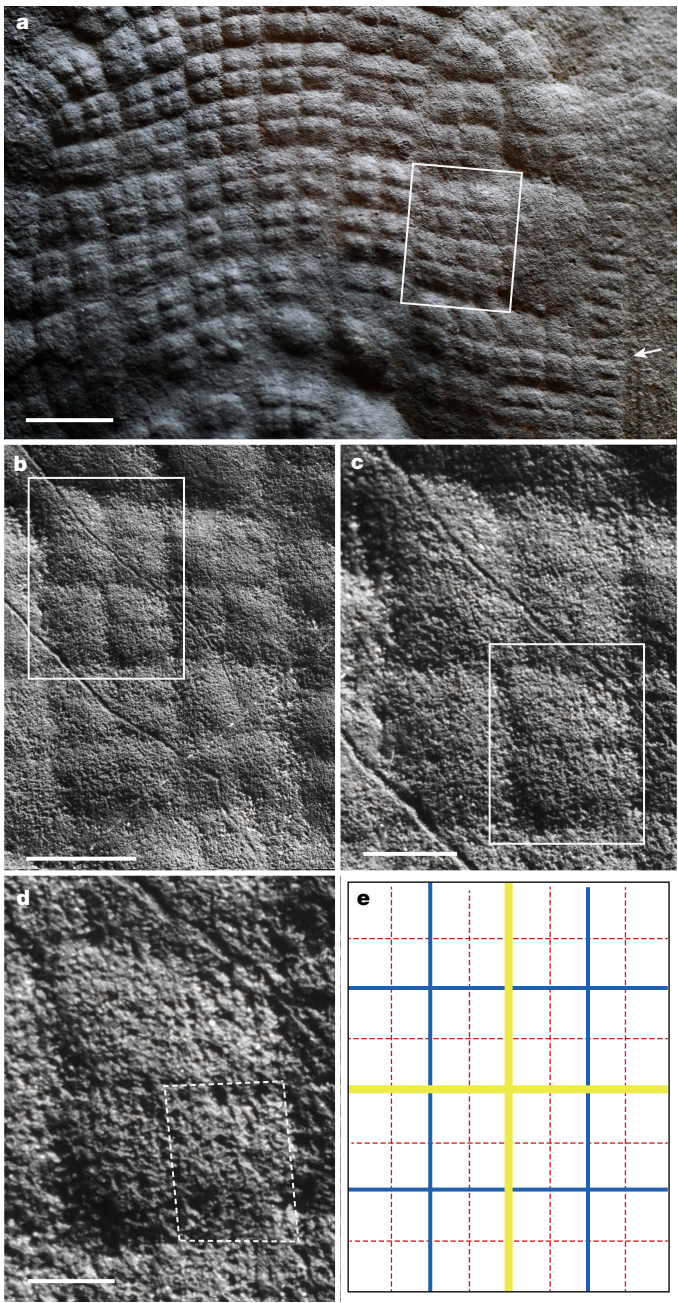


Fig. 2 | Hierarchical rectangles on the surface of *H. cantori* gen. et sp. nov., holotype, NIGP-176531. **a**, Upper part of the body preserved in positive epirelief, viewed under reflected light directed from the upper right. Arrow marks fringe-like structure. **b–d**, Negative hyporelief counterpart impression with a different lighting angle. **b**, First-order rectangle in **b** corresponds to box in **a**. **c**, Second-order rectangle in **c** corresponds to box in **b**. **d**, Third-order rectangle in **d** corresponds to box in **c**, with dashed box marking a faintly preserved fourth-order rectangle. **e**, Schematic diagram of hierarchical rectangles. Black box marks first-order rectangle. Yellow, blue and red lines represent grooves that divide first-, second- and third-order rectangles, respectively. Scale bars, 10 mm (**a**), 5 mm (**b**), 2 mm (**c**), 1 mm (**d**).

Discussion

The presence of a stem and a discoidal holdfast suggests an erect benthic lifestyle (Fig. 4a), but these features are not phylogenetically informative because they are also present in several distantly related benthic Ediacaran taxa, such as the putative cnidarian *Haootia*¹⁵, the macroalga *Discusphyton*²⁸, arboreomorphs²⁹ and some rangeomorphs

(for example, *Charnia*¹⁴ and *Primocandabrum*³⁰), as well as many extant sponges³¹, cnidarians³², fungi and various algae. Instead, the stem and holdfast probably represent a convergent adaptation to a benthic lifestyle on microbially bound, firm substrates, which were prevalent during the Ediacaran period and are inferred to be present in the Shibantan assemblages on the basis of dark, organic-rich crinkly laminations observed in thin sections from this unit³³. Common anchored benthic Ediacaran taxa such as *Charnia*³⁴ and *Arborea*³⁵ are leaf-like and constructed by branching modules, whereas *H. cantori* has a conical body consisting of a regular hierarchical latticework, evidencing a very different body plan and functional morphology.

The main body of *Helicolocellus* shares a conical to cylindrical morphology with late-Ediacaran taxa, which have previously been likened to sponges, but possesses sufficient morphological differences to justify the establishment of a new taxon based on the Shibantan material. The putative sponge *Thectardis*^{36,37} from Newfoundland is inferred to have possessed a conical body which is similar to *Helicolocellus*, but *Thectardis* typically shows a featureless external surface and lacks a stem or basal disc. Another cylindrical fossil, the putative sponge *Ausia* from the Nama Group of Namibia³⁸, has millimetre-scale pore-like structures on its surface, albeit notably smaller than the first-order rectangles observed in *H. cantori* and lacking second-order divisions. *Palaeophragmodictya*, a discoidal fossil found in South Australia and the White Sea region of Russia, was initially interpreted as a sponge³⁹ and shares reticulate surface patterns which are smaller than those of *H. cantori*. However, it differs markedly in shape, being discoidal rather than conical, and more recent research indicates that it may represent an attachment disc of frondose organisms or a microbially produced texture⁵. The Ediacaran fossil *Gibbavasis*^{40,41} from Iran and Moldova shares a lattice-like appearance with *Helicolocellus* but possesses only a single order of orthogonally arranged ‘boxes’. Furthermore, *Gibbavasis* is much smaller (4–14 mm long, 2–7 mm wide) than *Helicolocellus*. Perpendicular cross-hatched structures have also been described in an unnamed fossil from Nevada (Fig. 3a,b in ref. 42). However, its surface ornamentation can be readily distinguished from the reticulation observed in *H. cantori* by the absence of secondary latticework.

The box-like latticework pattern of *Helicolocellus* is superficially similar to the transverse and longitudinal furrows on the body walls of some living hexacorallians (Cnidaria: Anthozoa), such as stony corals (Scleractinia) and sea anemones (Actiniaria). In these hexacorallians, the furrows correspond to a latticework of internal muscle fibres known as a muscle field⁴³. However, the box-like structures in the Hexacorallia are not subdivided into finer units, nor are they arranged diagonally as in *Helicolocellus* and sponges. Furthermore, the irregular arrangement of boxes observed in some *Helicolocellus* specimens (for example, Figs. 1a and 3b) cannot be easily explained by disturbance of the contractile muscle field seen in the Hexacorallia. Contractile muscle fields are typically highly variable in length-to-width ratio, inconsistent with the relatively stable ratio of *Helicolocellus* specimens (around 3.0, measured on three specimens) in *Helicolocellus*. More importantly, tentacles are considered a synapomorphy (shared derived characteristic) of the Anthozoa⁴⁴ but are not present in *Helicolocellus*, thus excluding *Helicolocellus* from the total-group Hexacorallia. Similarities with the longitudinal and transverse muscle bundles of extant tunicates can also be refuted by the ability of *Helicolocellus* rectangles to behave as discrete individual blocks, which can result in irregular arrangement, particularly in the lower part of the conical body (Figs. 1a and 3b). The enigmatic Cambrian fossil *Paramackenzia*, which has previously been compared to modular Ediacaran organisms and exhibits potential three-dimensional box-like compartmental structures⁴⁵, has passing similarity, but its compartmental structures neither subdivide nor show a helical arrangement.

The body plan of *Helicolocellus*, with its goblet-like shape and especially the hierarchical rectangular ornament, is highly similar to the overall morphology and skeletal grid of Palaeozoic hexactinellid sponges, in which the pattern results from the presence of regularly arranged



Fig. 3 | More specimens of *H. cantorigen. et sp. nov.* **a**, Paratype, NIGP-176532, with the body preserved in negative epirelief and the associated stem and disc in positive epirelief. **b**, NIGP-176533, body preserved in positive relief, with irregular arrangement of rectangular boxes towards the base of the specimen. Stratigraphic orientation uncertain. Arrows indicate two regions where the stem width expands from 32 mm to 48 mm. **c**, Presumed juvenile specimen, NIGP-176536, showing a truncated distal end. The body is preserved in positive relief, whereas the stem is a negative relief impression. Stratigraphic orientation uncertain. Scale bars, 50 mm (**a,b**), 20 mm (**c**).

biomineralized spicules. For example, stem-group hexactinellids such as the Protospongiidae (Extended Data Fig. 3a,b) and the Dictyospongidae (Extended Data Fig. 3c,d) are characterized by similar regular and uniformly divided meshes of spicules⁴⁶. Dictyospongids, which are funnel-shaped or cylindrical sponges, can reach considerable sizes, with genera such as *Hydnoceras* growing larger than 250 mm (ref. 46). *Clathrosporgia* and *Minitaspongia* exhibit first-order meshes that are 1.5–15 mm wide and 2–15 mm long^{47,48}, which are comparable in size to those of *Helicolocellus*. In some cases, the orthogonal rays of spicules that form the skeletal grids and outline the ‘boxes’ in *Clathrosporgia* may appear as deep impressions as a result of the dissolution of spicules during diagenesis⁴⁸, resulting in a preservational style virtually identical to *Helicolocellus*. The protrusion of sediment through the spaces between the orthogonal rays may also result in a rectangular pattern⁴⁷ similar to that of *Helicolocellus*. Some other Cambrian sponges, for

example, the demosponge *Vauxia* and the ascospunge *Leptomitus*, also exhibit a grid pattern⁴⁹. However, these patterns differ significantly from the regular and hierarchical grid pattern found in *Helicolocellus* and other Palaeozoic hexactinellid sponges in having less hierarchy in their organization and less regularity in the spicule arrangements.

The hierarchical skeletal grid in these Palaeozoic hexactinellid sponges consists of multiscale bundles of spicules, typically either fused together or loosely assembled to form a latticework. Although *Helicolocellus* lacks direct evidence for a biomineralized skeleton, it probably had a somewhat rigid skeleton consisting of discrete cruciform elements, considering the presence of both regularly and irregularly arranged reticulate patterns in observed specimens. It is thus taphonomically similar to the Devonian fossil *Pontagrossia*⁵⁰ (Extended Data Fig. 3f), which has been compared to a sponge and is inferred to have possessed a largely organic skeleton characterized by a reticulate pattern. The skeleton of *Helicolocellus* could similarly have been originally organic, considering its taphonomic style similar to other non-biomineralized macrofossils such as *Arborea*²³, *Flabellphyton*²⁴ and *Wutubus*²⁵ but different from the biomineralized tubular fossil *Cloudina*²⁶ in the Shibantan Member. Additionally, the outwardly bulging upper surface of the rectangles in *Helicolocellus* (as evidenced by convex-up positive epirelief preservation, seen in the holotype) is consistent with a flexible wall or membrane which was pushed outward during sediment infilling and compaction and impressed against a more rigid external framework.

Some clusters of rectangles in *Helicolocellus* are irregularly arranged, particularly in the lower part of the conical body (Figs. 1a and 3b). These irregularly arranged rectangles may result from the dislocation of some rectangular elements during either degradation or compaction. Similar irregular arrangement is also observed in protospongiid sponges (Extended Data Fig. 3b), which are constructed of loosely articulated cruciform units known as stauractine spicules which are prone to postmortem dislocation⁵¹. This observation indicates that the skeleton of *Helicolocellus* was constructed of unfused skeletal elements. Considering the possibility that early Palaeozoic sponge spicules were weakly biomineralized and contained large proportions of organic matter, with full biomineralisation only seen in later sponges⁹, we might expect early sponges such as *Helicolocellus* to have organic, unfused skeletal elements prone to dislocation.

The attachment strategy of *Helicolocellus* can also find analogues among younger sponges. The Jurassic protospongiid-like sponge *Ammonella*, for example, shows a regular and hierarchical meshwork of stauractines⁴⁹, resembling the pattern observed in *Helicolocellus*, and was also anchored to a potentially microbially stabilized substrate by a discoid root plate⁵². This attachment strategy bears similarity to the way *Helicolocellus* adheres to the (presumably microbially stabilized⁵³) Ediacaran substrate.

To more rigorously test the possible hexactinellid affinity of *Helicolocellus*, a Bayesian phylogenetic analysis was conducted using a dataset consisting of 79 taxa (including 8 fossil taxa) and 235 characters, with 67 of these characters scored for *Helicolocellus* (see Supplementary Information for methods and details of the character matrix). Notably, *Helicolocellus* was assigned to have a highly regular hierarchical reticulate skeleton (character 176). The analysis recovers *Helicolocellus* as a crown-group sponge and a stem-group hexactinellid (Fig. 4b and Extended Data Fig. 4). This result is unsurprising given that all crown-group hexactinellids have biomineralized spicules⁵⁴ and *Helicolocellus* does not. Moreover, the Bayes factor (15.82) indicates a strong statistical support for a crown-group sponge placement of *Helicolocellus* over a stem-group Porifera alternative (Supplementary Information). The results remain stable in several sensitivity tests: when ctenophores are constrained as the sister-group to all other animals⁵⁵ (Extended Data Fig. 5a) and when the relationships of the classes in Porifera and the internal relationships in Hexactinellida are constrained to follow recent molecular phylogenies^{10,54} (Extended Data Fig. 5b).

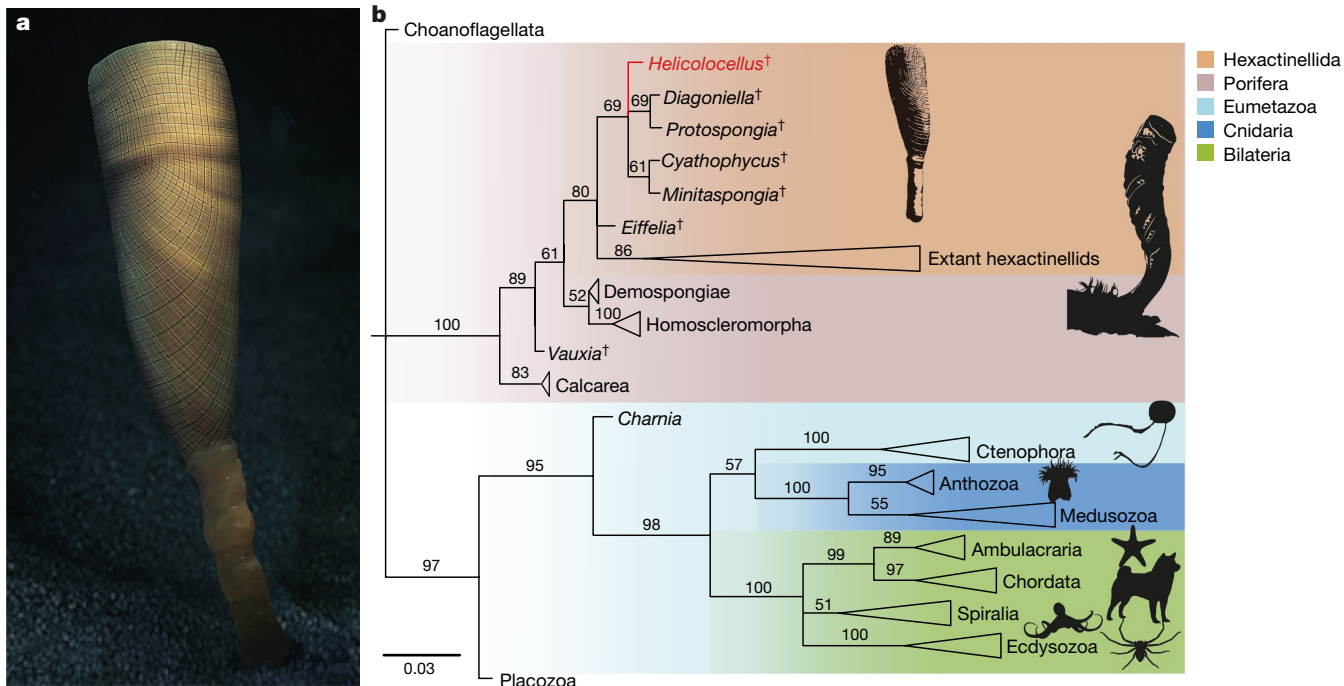


Fig. 4 | Morphological reconstruction and phylogenetic position of *H. cantorigen. et sp. nov.* **a**, Reconstructed life position of *H. cantorigen* on the Ediacaran seafloor. Artwork by D. Yang. **b**, Bayesian phylogenetic analysis of metazoans, based on character matrix modified from refs. 14, 54, 68. *H. cantorigen* is resolved as a stem-group hexactinellid along with *Eiffelia*, *Diagoniella*,

Protospongia, *Cyathophycus* and *Minitaspongia*. The total-group hexactinellid clade shows a basal polytomy of three branches: 1, *Helicocellus* and reticulosans; 2, *Eiffelia*; 3, crown-group or extant hexactinellids. Numbers are posterior probabilities for nodes. See Supplementary Information for morphological data matrix.

The latticework of *Helicocellus* may have facilitated feeding or mechanical stability. As in modern sponges and diploblastic animals, early sponges probably lacked specialized internal organs and may have depended on diffusion for gas exchange and osmotrophic or filter feeding^{32,56}. A simple and effective strategy to achieve these functions is to increase the ratio of surface area to volume, as occurs in several extant shallow-water sponges, in which organic particles and dissolved organic matter serve as a chief food source⁵⁷. Modern hexactinellid sponges possess a syncytial pinacoderm and a water canal system lined with choanocytes⁵⁸ (branched choanoderm). The various forms (for example, folding, branching and anastomosis) of hexactinellid skeletons have been interpreted as an adaptation to maximize the choanoderm surface area in the limited space occupied by the sponge⁵⁹. The repeatedly divided box pattern in *Helicocellus* may represent a similar strategy to increase surface area. This pattern resembles a self-similar fractal known as the Cantor dust set, which is generated through a recursive process of repeatedly inserting a central cross in rectangles, resulting in successively smaller rectangles which are geometrically similar to one another (Fig. 2). Fractals are ubiquitous in biology but appear almost exclusively in the form of branching tubes⁶⁰, such as in the lungs, leaf veins and plant roots. Non-branching fractals are exceedingly rare in organisms. The Cantor dust set is unique to *Helicocellus* and some Palaeozoic sponges. This multiscale hierarchical structure may also provide mechanical benefits; broadly similar skeletal systems in modern hexactinellid sponges, such as *Euplectella*, have been shown to contribute to mechanical stability⁶¹.

The overall morphology and regular grid-like pattern on the body wall of *Helicocellus* are consistent with an affinity with sponges, particularly hexactinellids. However, there are two key features of modern hexactinellids that are not observed in *Helicocellus*. First, the reticulation of modern hexactinellid sponges is typically constructed by cruciform stauract spicules bounded by soft tissue or by fused spicules, whereas no mineralized spicules have been found in

Helicocellus. This apparent absence is probably original, with any cruciform skeletal elements in *Helicocellus* being non-biomimeticized. The last common ancestor of sponges may have been aspiculate^{11–13}, and the siliceous spicules of the modern sponge classes—Hexactinellida, Demospongidae and Homoscleromorpha—have been shown not to be homologous¹³. Those sponge classes may have independently acquired mineralized skeletons along with other metazoan lineages in the early Cambrian^{10–13}. Palaeontological and molecular phylogenetic analyses have not arrived at a conclusive resolution with regard to the origin(s) of biomimeticization in sponges¹², with some studies advocating the origin of biomimeticized spicules in the last common ancestor of the Silicea⁶² or even Porifera⁶ and others entertaining the possibility of independent origins of siliceous spicules in the Hexactinellida, Demospongidae and Homoscleromorpha^{9,13,63}. Our phylogenetic placement of *Helicocellus* as a stem-group hexactinellid that possesses some (for example, a reticulate skeleton) but not all (for example, biomimeticized spicules) features of the crown-group Hexactinellida is consistent with either independent origins or secondary loss of siliceous spicules. Second, the surface of *Helicocellus* lacks evidence for ostia (inhaltant pores). It is possible that the minute size of ostia, such as those observed in extant hexactinellid sponges (for example, 4–30 µm; ref. 64) may not have been preserved in this deposit. The smallest resolvable features preserved in the Shabantan limestone are tertiary branches of *Charnia*, which have a submillimeter minimum dimension (ref. 65), an order of magnitude larger than would be predicted for ostia. Our ability to determine the presence of an osculum-like structure in *Helicocellus* is hampered by the lateral compression of all specimens at hand, but the three-dimensional cement-filled cross-section through the holotype (Fig. 1c) suggests the likely presence of a central cavity in *Helicocellus*, which could be homologous to the spongocoel in modern sponges.

It is also worth commenting on the phylogenetic placement of the hexactine-bearing Reticulosa, which has traditionally been assigned to the hexactinellids⁶⁶ but has since been proposed to be paraphyletic to

the Hexactinellida, Demospongiae, Calcarea and Homoscleromorpha and even the entire Porifera⁶. Our phylogenetic analysis indicates that at least some extinct reticulosan taxa, that is, *Diagoniella*, *Protospongia*, *Eiffelia*, *Cyathophycus* and *Minitaspongia*, along with the heteractinid *Eiffelia*, are grouped with extant hexactinellids (Fig. 4b). Therefore, reticulosan and heteractinid sponges may represent stem-group hexactinellids.

To conclude, *H. cantori* represents an Ediacaran crown-group sponge with an organic skeleton that is architecturally similar to the Hexactinellida. If siliceous biomineralization evolved independently in the Hexactinellida, Demospongiae and Homoscleromorpha¹³, then a pre-existing organic scaffold with a regular hierarchical reticulate skeleton (as present in *H. cantori*) may have served as a template for subsequent acquisition of biomineralized spicules. An important ramification is that we should broaden our search image of Precambrian sponge fossils, not only because they may have been aspiculate if sponge biomineralization evolved several times (for example, Tonian candidate keratose sponge material from Canada⁷) but also because stem-group representatives necessarily lacked some features diagnostic of their crown-group counterparts^{6,7}. This emphasizes the phylogenetic importance of the fossil record in the search of the evolutionary root of sponges and indeed all animals.

Online content

Any methods, additional references, Nature Portfolio reporting summaries, source data, extended data, supplementary information, acknowledgements, peer review information; details of author contributions and competing interests; and statements of data and code availability are available at <https://doi.org/10.1038/s41586-024-07520-y>.

- Redmond, A. K. & Mclysaght, A. Evidence for sponges as sister to all other animals from partitioned phylogenomics with mixture models and recoding. *Nat. Commun.* **12**, 1783 (2021).
- Lenton, T. M., Boyle, R. A., Poulton, S. W., Shields-Zhou, G. A. & Butterfield, N. J. Co-evolution of eukaryotes and ocean oxygenation in the Neoproterozoic era. *Nat. Geosci.* **7**, 257–265 (2014).
- dos Reis, M. et al. Uncertainty in the timing of origin of animals and the limits of precision in molecular timescales. *Curr. Biol.* **25**, 2939–2950 (2015).
- Dohrmann, M. & Wörheide, G. Dating early animal evolution using phylogenomic data. *Sci. Rep.* **7**, 3599 (2017).
- Antcliffe, J. B., Callow, R. H. T. & Brasier, M. D. Giving the early fossil record of sponges a squeeze. *Biol. Rev.* **89**, 972–1004 (2014).
- Botting, J. P. & Muir, L. A. Early sponge evolution: a review and phylogenetic framework. *Paleoworld* **27**, 1–29 (2018).
- Turner, E. C. Possible poriferan body fossils in early Neoproterozoic microbial reefs. *Nature* **596**, 87–91 (2021).
- Neuweiler, F. et al. Keratose sponges in ancient carbonates—a problem of interpretation. *Sedimentology* **70**, 927–968 (2023).
- Tang, Q., Wan, B., Yuan, X., Muscente, A. D. & Xiao, S. Spiculogenesis and biomimetic mineralization in early sponge animals. *Nat. Commun.* **10**, 3348 (2019).
- Aguilar-Camacho, J. M., Doonan, L. & McCormack, G. P. Evolution of the main skeleton-forming genes in sponges (phylum Porifera) with special focus on the marine Haplosclerida (class Demospongiae). *Mol. Phylogenet. Evol.* **131**, 245–253 (2019).
- Murdock, D. J. E. The ‘biomineralization toolkit’ and the origin of animal skeletons. *Biol. Rev.* **95**, 1372–1392 (2020).
- Xiao, S. Ediacaran sponges, animal biomineralization and skeletal reefs. *Proc. Natl Acad. Sci. USA* **117**, 20997–20999 (2020).
- Shimizu, K. et al. Silica-associated proteins from hexactinellid sponges support an alternative evolutionary scenario for biomineralization in Porifera. *Nat. Commun.* **15**, 181 (2024).
- Dunn, F. S. et al. The developmental biology of *Charnia* and the eumetazoan affinity of the Ediacaran rangeomorphs. *Sci. Adv.* **7**, eabe0291 (2021).
- Liu, A. G., Matthews, J. J., Menon, L. R., McIlroy, D. & Brasier, M. D. *Haootia quadriformis* n. gen., n. sp., interpreted as a muscular cnidarian impression from the Late Ediacaran period (approx. 560 Ma). *Proc. R. Soc. B* **281**, 20141202 (2014).
- Dunn, F. S. et al. A crown-group cnidarian from the Ediacaran of Charnwood Forest, UK. *Nat. Ecol. Evol.* **6**, 1095–1104 (2022).
- Chen, Z., Zhou, C., Yuan, X. & Xiao, S. Death march of a segmented and trilobate bilaterian elucidates early animal evolution. *Nature* **573**, 412–415 (2019).
- Love, G. D. et al. Fossil steroids record the appearance of Demospongiae during the Cryogenian period. *Nature* **457**, 718–721 (2009).
- Nettersheim, B. J. et al. Putative sponge biomarkers in unicellular Rhizaria question an early rise of animals. *Nat. Ecol. Evol.* **3**, 577–581 (2019).
- Zumberge, J. A. et al. Demosponge steroid biomarker 26-methylstigmastane provides evidence for Neoproterozoic animals. *Nat. Ecol. Evol.* **2**, 1709–1714 (2018).
- Muscente, A. D., Marc Michel, F., Dale, J. G. & Xiao, S. Assessing the veracity of Precambrian ‘sponge’ fossils using in situ nanoscale analytical techniques. *Precambrian Res.* **263**, 142–156 (2015).
- Sperling, E. A., Robinson, J. M., Pisani, D. & Peterson, K. J. Where’s the glass? Biomarkers, molecular clocks and microRNAs suggest a 200-Myr missing Precambrian fossil record of siliceous sponge spicules. *Geobiology* **8**, 24–36 (2010).
- Wang, X. et al. The Ediacaran frondose fossil Arborea from the Shibanian limestone of South China. *J. Paleontol.* **94**, 1034–1050 (2020).
- Wan, B. et al. A tale of three taphonomic modes: the Ediacaran fossil *Flabellophyton* preserved in limestone, black shale and sandstone. *Gondwana Res.* **84**, 296–314 (2020).
- Chen, Z. et al. New Ediacara fossils preserved in marine limestone and their ecological implications. *Sci. Rep.* **4**, 4180 (2014).
- Chen, X., Zhou, P., Zhang, B., Wei, K. & Zhang, M. Lithostratigraphy, biostratigraphy, sequence stratigraphy and carbon isotope chemostratigraphy of the upper Ediacaran in Yangtze Gorges and their significance for chronostratigraphy. *South China Geol.* **32**, 87–105 (2016).
- Yang, B., Warren, L. V., Steiner, M., Smith, E. F. & Liu, P. Taxonomic revision of Ediacaran tubular fossils: *Cloudina*, *Sinotubulites* and *Conotubus*. *J. Paleontol.* **96**, 256–273 (2022).
- Wang, Y., Wang, Y. & Du, W. A rare disc-like holdfast of the Ediacaran macroalga from South China. *J. Paleontol.* **91**, 1091–1101 (2017).
- Laflamme, M., Gehling, J. G. & Droser, M. L. Deconstructing an Ediacaran frond: three-dimensional preservation of Arborea from Ediacara, South Australia. *J. Paleontol.* **92**, 323–335 (2018).
- Hofmann, H. J., O’Brien, S. J. & King, A. F. Ediacaran biota on Bonavista Peninsula, Newfoundland, Canada. *J. Paleontol.* **82**, 1–36 (2008).
- Mitchell, E. G. & Harris, S. Mortality, population and community dynamics of the glass sponge dominated community “The Forest of the Weird” from the Ridge Seamount, Johnston Atoll, Pacific Ocean. *Front. Mar. Sci.* **7**, 565171 (2020).
- Brusca, R. C., Moore, W. & Shuster, S. M. *Invertebrates* (Sinauer Associates, 2016).
- Xiao, S., Shen, B., Zhou, C., Xie, G. & Yuan, X. A uniquely preserved Ediacaran fossil with direct evidence for a quilted bodyplan. *Proc. Natl Acad. Sci. USA* **102**, 10227–10232 (2005).
- Ford, T. D. Pre-Cambrian fossils from Charnwood Forest. *Proc. Yorks. Geol. Soc.* **31**, 211–217 (1958).
- Glaessner, M. F. & Daily, B. The geology and Late Precambrian fauna of the Ediacara fossil reserve. *Rec. South Aust. Mus.* **13**, 369–401 (1959).
- Clapham, M. E., Narbonne, G. M., Gehling, J. G., Greenacre, C. & Anderson, M. M. *Thectardis avalonensis*: a new Ediacaran fossil from the Mistaken Point biota, Newfoundland. *J. Paleontol.* **78**, 1031–1036 (2004).
- Sperling, E. A., Peterson, K. J. & Laflamme, M. Rangeomorphs, *Thectardis* (Porifera?) and dissolved organic carbon in the Ediacaran oceans. *Geobiology* **9**, 24–33 (2011).
- Hahn, G. & Pflug, H. D. Polypenartige Organismen aus dem Jung-Präkambrium (Nama-Gruppe) von Namibia. *Geol. Palaeontol.* **19**, 1–13 (1985).
- Gehling, J. G. & Rigby, J. K. Long expected sponges from the Neoproterozoic Ediacara fauna of South Australia. *J. Paleontol.* **70**, 185–195 (1996).
- Francovschi, I., Grădinaru, E., Li, H., Shumlyansky, L. & Ciobotaru, V. U-Pb geochronology and Hf isotope systematics of detrital zircon from the late Ediacaran Kalyus Beds (East European Platform): palaeogeographic evolution of southwestern Baltica and constraints on the Ediacaran biota. *Precambrian Res.* **355**, 106062 (2021).
- Vaziri, S. H., Majidifard, M. R. & Laflamme, M. Diverse assemblage of Ediacaran fossils from Central Iran. *Sci. Rep.* **8**, 5060 (2018).
- Smith, E. F., Nelson, L. L., Tweedt, S. M., Zeng, H. & Workman, J. B. A cosmopolitan late Ediacaran biotic assemblage: new fossils from Nevada and Namibia support a global biostratigraphic link. *Proc. R. Soc. B* **284**, 20170934 (2017).
- McMahon, S., Tarhan, L. G. & Briggs, D. E. G. Decay of the sea anemone *Metridium* (Actiniaria): implications for the preservation of cnidarian polyps and other soft-bodied diploblast-grade animals. *Palaios* **32**, 388–395 (2017).
- Ou, Q. et al. Dawn of complex animal food webs: a new predatory anthozoan (Cnidaria) from Cambrian. *Innovation* **3**, 100195 (2022).
- Zhao, Y. et al. An early Cambrian mackenziaid reveals links to modular Ediacaran macro-organisms. *Palaeontol. Pap.* **14**, e1412 (2022).
- Hall, J. & Clarke, J. M. *A Memoir on the Palaeozoic Reticulate Sponges: Constituting the Family Dictyospongidae* (Wynkoop Hallenbeck Crawford Company, 1898).
- Carrera, M., Rustan, J., Vaccari, N. & Ezpeleta, M. A Mississippian hexactinellid sponge from the Western Gondwana: taxonomic and paleobiogeographic implications. *Acta Palaeontol. Pol.* **63**, 63–70 (2018).
- Rigby, J. K. & Keyes, R. First report of hexactinellid dictyosponges and other sponges from the Upper Mississippian Bangor Limestone, northwestern Alabama. *J. Paleontol.* **64**, 886–897 (1990).
- Finks, R. M., Reid, R. E. H. & Rigby, J. K. *Treatise on Invertebrate Paleontology Part E (Revised)* (Geological Society of America and the University of Kansas, 2004).
- Chahud, A. & Fairchild, T. R. A new invertebrate from the Ponta Grossa Formation (Devonian), Paraná Basin, Brazil. *Rev. Bras. Paleontol.* **23**, 279–282 (2020).
- Wulff, J. in *Coral Reefs at the Crossroads* (eds Hubbard, D. K. et al.) 103–126 (Springer, 2016).
- Keupp, H. & Schweigert, G. *Neochoiaella* n. gen. (Demospongiae, Choiaellidae)—a second poriferan Lazarus taxon from the Solnhofen Plattenkalk (Upper Jurassic, Southern Germany)? *Paläontol. Z.* **86**, 269–274 (2012).
- Bottjer, D. J., Hagadorn, J. W. & Dornbos, S. Q. The Cambrian substrate revolution. *GSA Today* **10**, 1–7 (2000).
- Dohrmann, M., Janussen, D., Reitner, J., Collins, A. G. & Wörheide, G. Phylogeny and evolution of glass sponges (Porifera, Hexactinellida). *Syst. Biol.* **57**, 388–405 (2008).
- Dunn, C. W., Leys, S. P. & Haddock, S. H. D. The hidden biology of sponges and ctenophores. *Trends Ecol. Evol.* **30**, 282–291 (2015).

56. Schlichter, D. in *Biology of the Integument: Invertebrates* (eds Bereiter-Hahn, J. et al.) 79–95 (Springer, 1984).
57. de Goeij, J. M., Lesser, M. P. & Pawlik, J. R. in *Climate Change, Ocean Acidification and Sponges: Impacts Across Multiple Levels of Organization* (eds Carballo, J. L. & Bell, J. J.) 373–410 (Springer, 2017).
58. Leys, S. P., Mackie, G. O. & Reiswig, H. M. The biology of glass sponges. *Adv. Mar. Biol.* **52**, 1–145 (2007).
59. Finks, R. M. in *Series in Geology, Notes for Short Course* (ed. Broadhead, T. W.) 101–115 (Univ. Tennessee, 1983).
60. Nonnenmacher, T. F., Losa, G. A. & Weibel, E. R. *Fractals in Biology and Medicine* (Birkhäuser, 2013).
61. Weaver, J. C. et al. Hierarchical assembly of the siliceous skeletal lattice of the hexactinellid sponge *Euplectella aspergillum*. *J. Struct. Biol.* **158**, 93–106 (2007).
62. Riesgo, A., Maldonado, M., López-Legentil, S. & Giribet, G. A proposal for the evolution of cathepsin and silicatein in sponges. *J. Mol. Evol.* **80**, 278–291 (2015).
63. Hill, M. S. et al. Reconstruction of family-level phylogenetic relationships within Demospongiae (Porifera) using nuclear encoded housekeeping genes. *PLoS ONE* **8**, e50437 (2013).
64. Mackie, G. O., Singla, C. L. & Smith, J. E. Studies on hexactinellid sponges. I. Histology of *Rhabdocalyptus dawsoni* (Lambe, 1873). *Philos. Trans. R. Soc. Lond. B* **301**, 365–400 (1983).
65. Wu, C. et al. The rangeomorph fossil *Charnia* from the Ediacaran Shibanian biota in the Yangtze Gorges area, South China. *J. Paleontol.* <https://doi.org/10.1017/jpa.2022.97> (2022).
66. Reid, R. E. H. A monograph of the Upper Cretaceous Hexactinellida of Great Britain and Northern Ireland Part I. *Monogr. Palaeontogr. Soc.* **111**, 1–46 (1958).
67. Xiao, S. Extinctions, morphological gaps, major transitions, stem groups and the origin of major clades, with a focus on early animals. *Acta Geol. Sin. Engl. Ed.* **96**, 1821–1829 (2022).
68. Manuel, M. et al. Phylogeny and evolution of calcareous sponges: monophly of calcinea and calcaronea, high level of morphological homoplasy and the primitive nature of axial symmetry. *Syst. Biol.* **52**, 311–333 (2003).

Publisher's note Springer Nature remains neutral with regard to jurisdictional claims in published maps and institutional affiliations.

Springer Nature or its licensor (e.g. a society or other partner) holds exclusive rights to this article under a publishing agreement with the author(s) or other rightsholder(s); author self-archiving of the accepted manuscript version of this article is solely governed by the terms of such publishing agreement and applicable law.

© The Author(s), under exclusive licence to Springer Nature Limited 2024

Article

Methods

Fossil specimens were collected from a single stratigraphic horizon about 2–2.5 m above the base of the Shibantan Member (around 551–543 Ma) at Wuhe village in the Yangtze Gorges area, South China (Extended Data Fig. 1). All specimens are preserved on limestone bedding surfaces and are deposited at the NIGP, Nanjing, China. Photographs were taken using a Nikon D850 DSLR camera and a Zeiss Axio Zoom V16 microscope. Measurements were carried out on fossil images using ImageJ 1.52a and analysed using Microsoft Excel 2013. Laser scanning data (Fig. 1b) were obtained using the Faro Design ScanArm and processed using the software Geomagic Warp 2017 and CloudCompare 2.13 to capture surface details and to generate elevation maps.

Phylogenetic analysis was conducted on the basis of a previously published character matrix for metazoans^{14,54,68} with modifications. No statistical methods were used to predetermine sample size. A total of 235 morphological characters were coded for 79 taxa. Only characters that are parsimony-informative were included in the analysis, to accentuate shared derived characters (synapomorphies). We scored *H. cantori* for 67 of these morphological characters (see Supplementary Information for details). Bayesian phylogenetic analysis was run using MrBayes 3.2.7 (ref. 69) on the CIPRES Science Gateway⁷⁰. Analyses were run for 6,000,000 generations, sampled with a frequency of every 1,000 generations, discarding the first 25% samples as burn-in. The average standard deviation of split frequencies was about 0.01 in all runs. The effective sample size, calculated using Tracer 1.7 (ref. 71), indicated that all parameters had effective sample size scores above 200.

We compared the Mk model with gamma and lognormal distributions, considering both symmetric and asymmetric transition frequencies. Additionally, we evaluated the topological hypotheses, specifically whether *Helicolocellus* is a stem-group sponge or a stem-group hexactinellid. To assess the strength of support for different models and hypotheses, we calculated marginal likelihoods, which were computed using stepping-stone sampling with 50 steps and 20,000,000 generations. The marginal likelihoods for each model were used to calculate Bayes factors and to determine the best-fit model⁷². Hard constraints were applied to all nodes during the stepping-stone sampling analysis for the two hypotheses. The results revealed that the model with a lognormal distribution and asymmetrical transition frequencies and the topology of the stem-group hexactinellid hypothesis were better supported (Supplementary Information and Supplementary Table 1). Therefore, the model with a lognormal distribution and asymmetrical transition frequencies was used in downstream analyses, as presented in Fig. 4b and Extended Data Fig. 4.

Reporting summary

Further information on research design is available in the Nature Portfolio Reporting Summary linked to this article.

Data availability

Fossils illustrated in this paper are accessioned in the NIGP (catalogue nos. NIGP-176531 to NIGP-176538, NIGP-155870, NIGP-201942).

Data collected or generated during this study are included in this article and its Supplementary Information. The nomenclature of *H. cantori* gen. et sp. nov. is registered in zoobank and the Life Science Identifier for this publication is urn:lsid:zoobank.org:pub:06F779B0-BA00-41AF-A6F7-A552BA8F6BF1.LSID.

69. Huelsenbeck, J. P. & Ronquist, F. MRBAYES: Bayesian inference of phylogenetic trees. *Bioinformatics* **17**, 754–755 (2001).
70. Miller, M. A., Pfeiffer, W. & Schwartz, T. Creating the CIPRES Science Gateway for inference of large phylogenetic trees. In 2010 *Gateway Computing Environments Workshop (GCE)* <https://doi.org/10.1109/GCE.2010.5676129> (IEEE, 2010).
71. Rambaut, A., Drummond, A. J., Xie, D., Baele, G. & Suchard, M. A. posterior summarization in Bayesian phylogenetics using Tracer 1.7. *Syst. Biol.* **67**, 901–904 (2018).
72. Ronquist, F., Huelsenbeck, J., Teslenko, M., Zhang, C. & Nylander, J. Draft MrBayes version 3.2 manual: tutorials and model summaries. *GitHub* https://github.com/NBISweden/MrBayes/blob/develop/doc/manual/Manual_MrBayes_v3.2.pdf (2020).
73. Xiao, S., Chen, Z., Pang, K., Zhou, C. & Yuan, X. The Shibantan Lagerstätte: insights into the Proterozoic–Phanerozoic transition. *J. Geol. Soc.* **178**, 2020–2135 (2021).
74. Condon, D. et al. U-Pb Ages from the Neoproterozoic Doushantuo Formation, China. *Science* **308**, 95–98 (2005).
75. Huang, T., Chen, D., Ding, Y., Zhou, X. & Zhang, G. SIMS U-Pb zircon geochronological and carbon isotope chemostratigraphic constraints on the Ediacaran–Cambrian boundary succession in the Three Gorges area, South China. *J. Earth Sci.* **31**, 69–78 (2020).
76. Okada, Y. et al. New chronological constraints for Cryogenian to Cambrian rocks in the Three Gorges, Weng'an and Chengjiang areas, South China. *Gondwana Res.* **25**, 1027–1044 (2014).
77. An, Z. et al. Stratigraphic position of the Ediacaran Miaohe biota and its constrains on the age of the upper Doushantuo $\delta^{13}\text{C}$ anomaly in the Yangtze Gorges area, South China. *Precambrian Res.* **271**, 243–253 (2015).
78. Xiao, S., Bykova, N., Kovalick, A. & Gill, B. C. Stable carbon isotopes of sedimentary kerogens and carbonaceous macrofossils from the Ediacaran Miaohe Member in South China: implications for stratigraphic correlation and sources of sedimentary organic carbon. *Precambrian Res.* **302**, 171–179 (2017).
79. Zhou, C. et al. The stratigraphic complexity of the middle Ediacaran carbon isotopic record in the Yangtze Gorges area, South China and its implications for the age and chemostratigraphic significance of the Shuram excursion. *Precambrian Res.* **288**, 23–38 (2017).
80. Liu, Q., Huang, D. & Gong, Y. Sponge fossils from the Cambrian Mantou Formation of Hebi, Henan, Central China. *J. China Univ. Geosci.* **37**, 129–135 (2012).
81. Virtual Collection (Digital Atlas of Ancient Life, accessed 23 April 2024); [www.digitalatlasofancientlife.org/vc/](http://digitalatlasofancientlife.org/vc/).

Acknowledgements This research was supported by Science Fund for Creative Research Groups of National Natural Science Foundation of China (41921002, 42130207, 41972005, 42272005), National Key R&D Program of China (2022YFF0800100, 2022YFF0802700) and the US National Science Foundation (EAR-2021207 to S.X.). We thank J. Li and W. Yang for help in fossil excavation; W. Yuan and Y. Chen for assistance with laser scanning; G. Mussini for assistance with phylogenetic analyses; and N. Butterfield, Z. Zhao and X. Xian for useful discussions.

Author contributions X.Y., S.X., Z.C., X.W. and B.W. designed the study. X.W., S.X., A.G.L., Z.C., X.Y. and B.W. interpreted the data. Z.C. coordinated the fieldwork. X.W. performed the phylogenetic analyses, compiled data and figures and composed the first draft of the manuscript with substantial contributions from S.X., A.G.L. and all co-authors.

Competing interests The authors declare no competing interests.

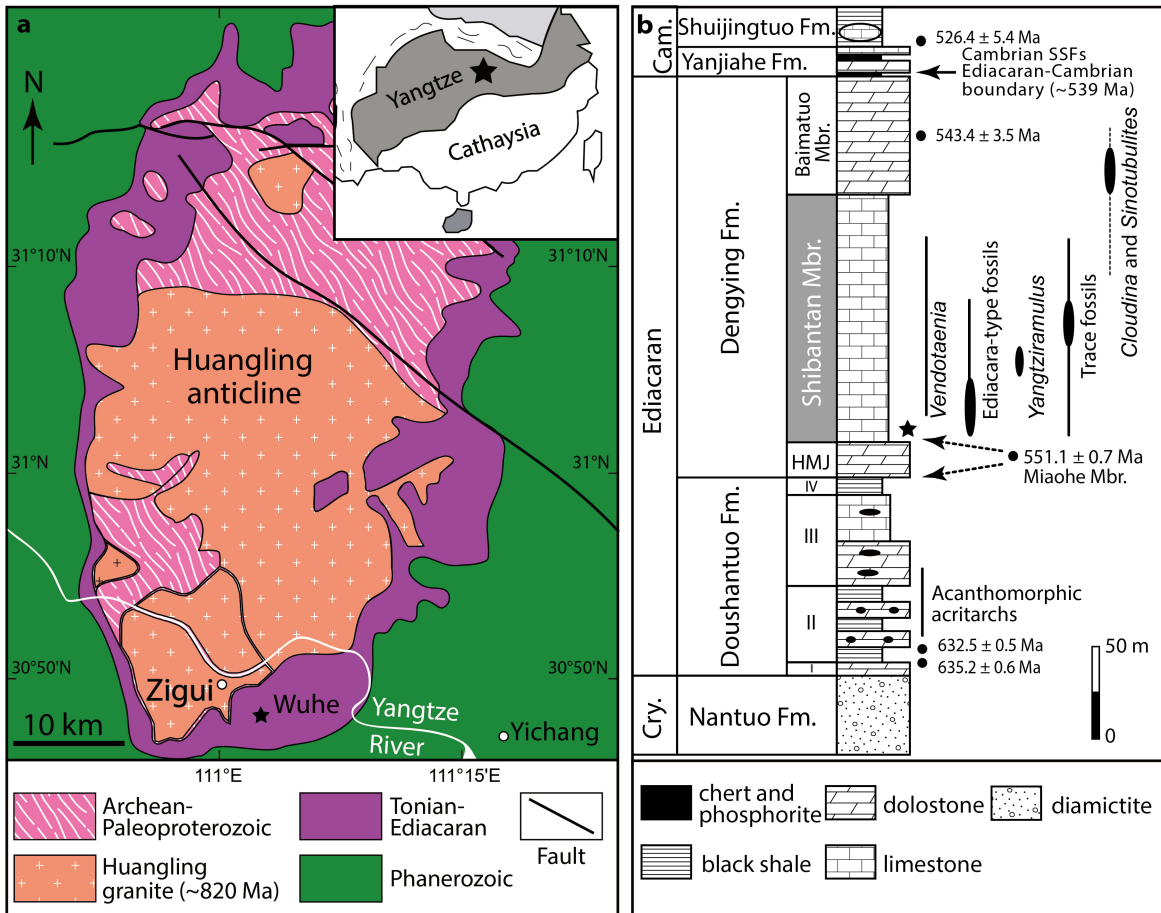
Additional information

Supplementary information The online version contains supplementary material available at <https://doi.org/10.1038/s41586-024-07520-y>.

Correspondence and requests for materials should be addressed to Bin Wan, Xunlai Yuan or Shuhai Xiao.

Peer review information *Nature* thanks Marc Laflamme, Lucy Muir and the other, anonymous, reviewer(s) for their contribution to the peer review of this work. Peer reviewer reports are available.

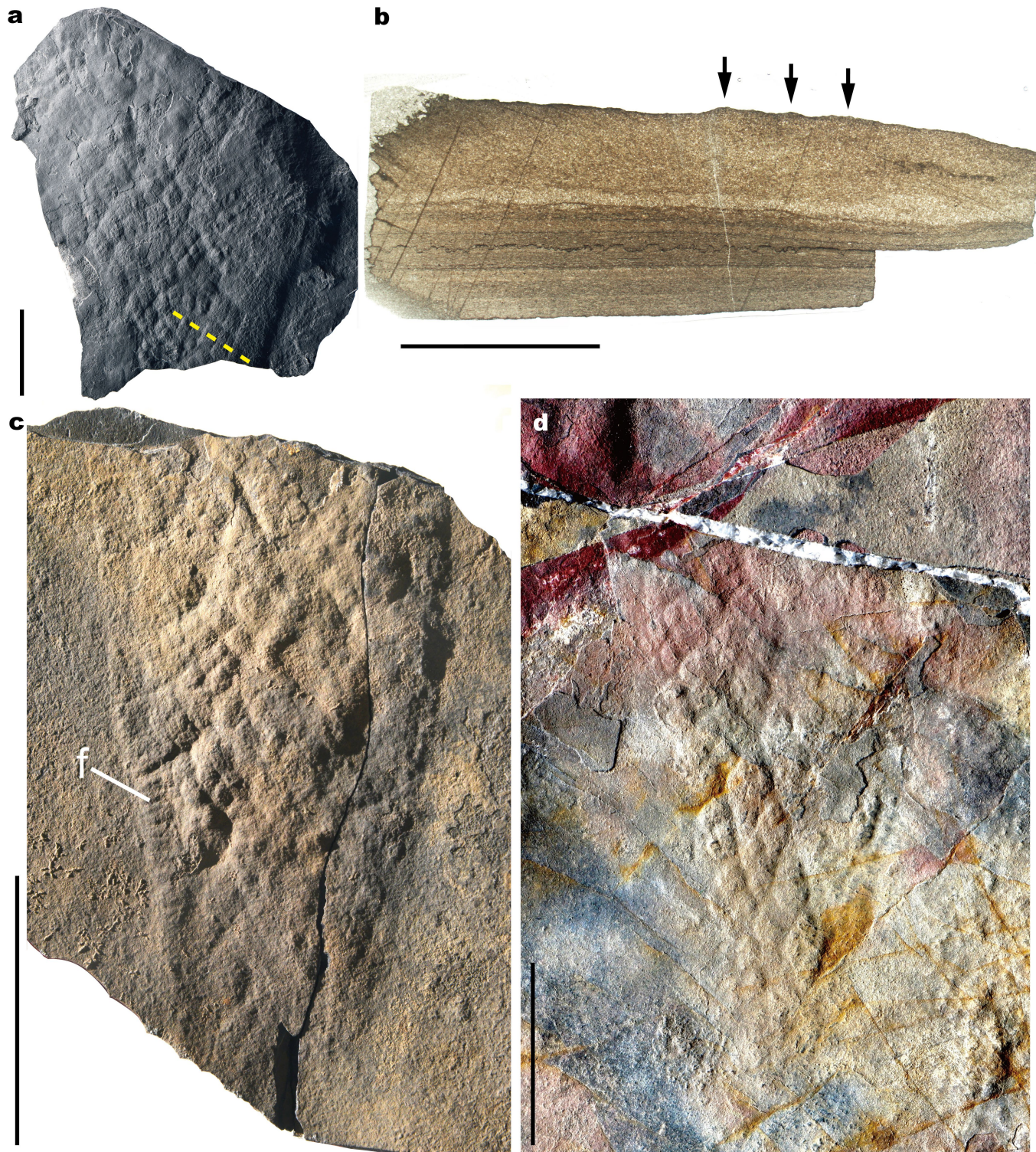
Reprints and permissions information is available at <http://www.nature.com/reprints>.



Extended Data Fig. 1 | Geological map and stratigraphic column. Star in **a** marks fossil locality on the southern margin of the Huangling anticline. Star in the inset map marks the location of the Huangling anticline on the South China block. Star in **b** shows the stratigraphic level from which *Helicolocellus* was discovered. Reproduced from Xiao, S., Chen, Z., Pang, K., Zhou, C. & Yuan, X. The Shihantan Lagerstätte: Insights into the Proterozoic–Phanerozoic transition.

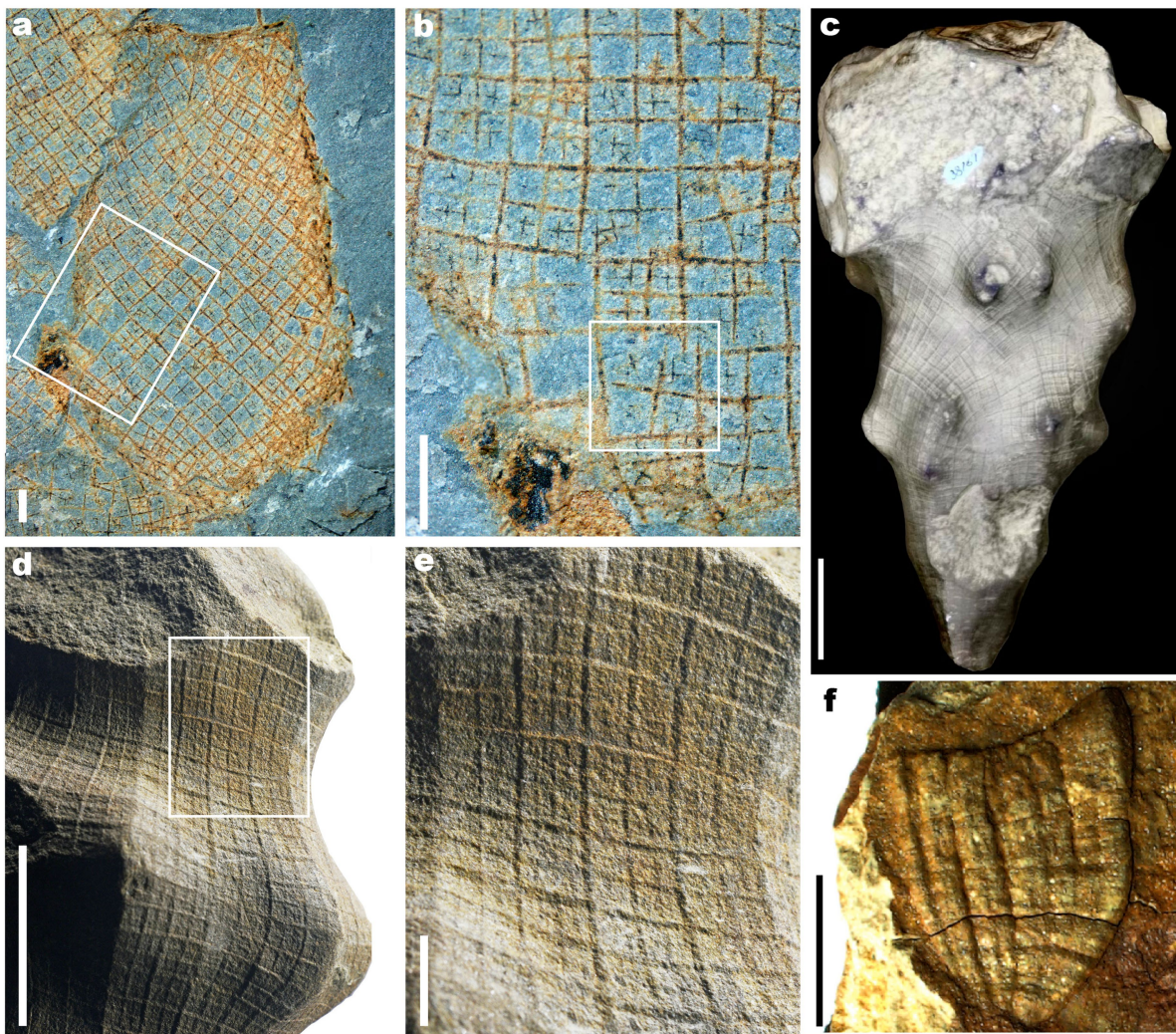
J. Geol. Soc. London 178, jgs2020-135 (2020) <https://doi.org/10.1144/jgs2020-135> (ref. 73). Sources of geochronometric data: 551.1 ± 0.7 Ma, 632.5 ± 0.5 and 635.2 ± 0.6 Ma from Condon et al.⁷⁴; 543.4 ± 3.5 Ma from Huang et al.⁷⁵; and 526.4 ± 5.4 Ma from Okada et al.⁷⁶. Dashed arrows indicate alternative correlations of the radiometric date from the Miaohe Member^{77–79}. Cam. = Cambrian; Cry. = Cryogenian; Fm. = Formation; HMJ = Hamajing Member; Mbr. = Member.

Article



Extended Data Fig. 2 | Additional specimens of *Helicoloceillus cantori* gen. et sp. nov. **a**, Positive relief of NIGP-176534. Stratigraphic orientation uncertain. Note irregular arrangement of boxes. **b**, Thin section perpendicular to bedding plane and along dashed line in **a**, showing boundaries of first order

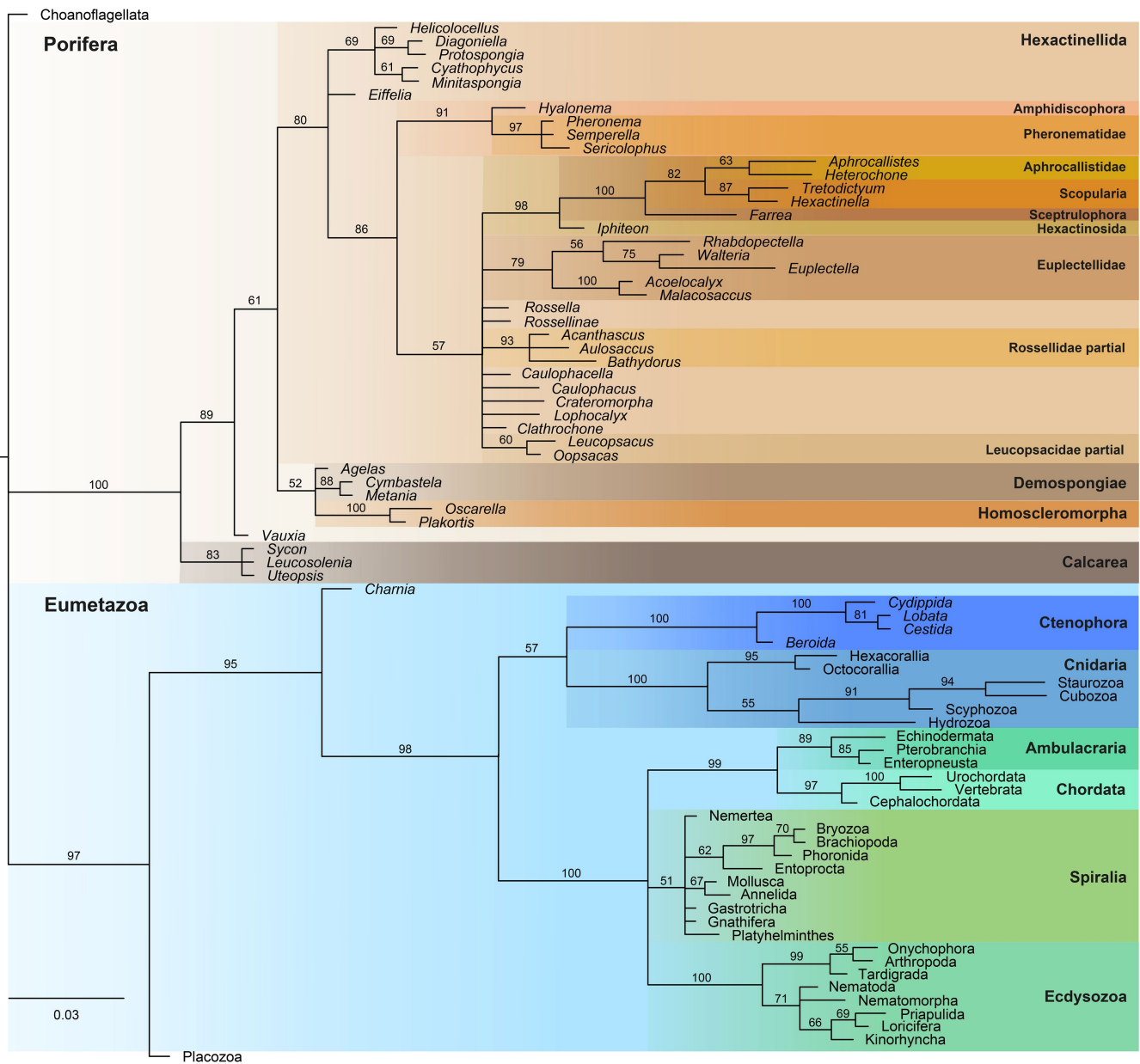
rectangles (arrowed). **c**, Positive relief on bed sole, NIGP-176535, showing fine grooves along the fringe of specimen. **d**, Positive relief on bed sole, NIGP-176538. **f**, fringe. Scale bars, 30 mm (**a**, **d**), 10 mm (**b**), 50 mm (**c**).



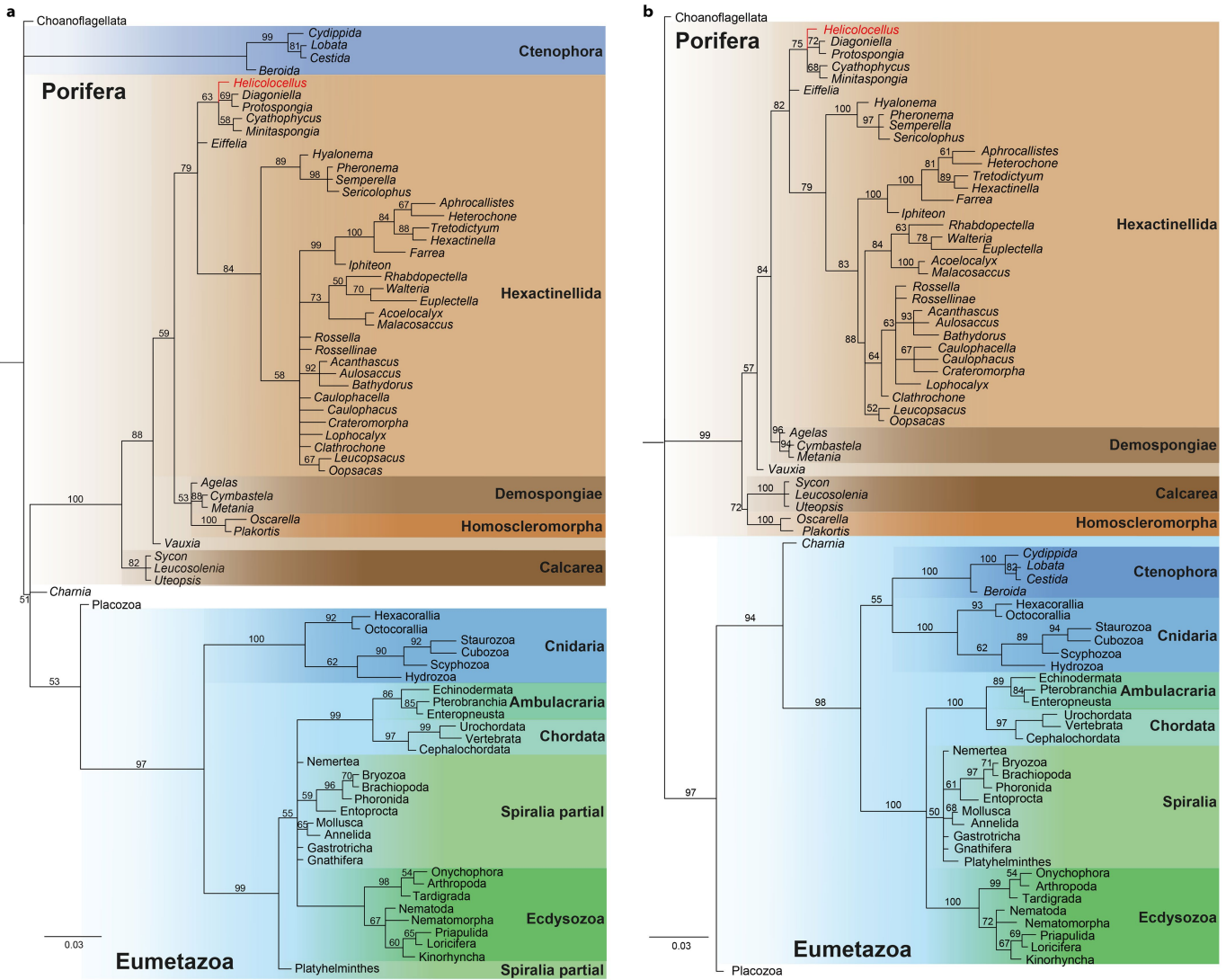
Extended Data Fig. 3 | Palaeozoic sponges and candidate sponges with skeletons organized in hierarchical latticework. **a**, Pyritized protospongiid *Diagoniella*, NIGP-155870, from the Mantou Formation of Henan Province, Wuliuan Stage (Cambrian)⁸⁰. **b**, Magnification of box in **a**. Box in **b** marks dislocated spicules. **c**, Devonian *Hydnoceras*, PRI 76741 (Digital Atlas of Ancient Life of the Paleontological Research Institution, Ithaca, New York⁸¹; license

CC0 1.0), showing helically arranged skeletal tracts. **d**, *Hydnoceras*, NIGP-201942, from the Upper Devonian Chemung Formation of New York. **e**, Magnification of the box in **d**, showing impressions of spicules. **f**, Devonian sponge-like fossil *Pontagrossia*⁵⁰, from the Ponta Grossa Formation of Paraná State (image provided by Artur Chahud and Thomas Fairchild). Scale bars, 1 mm (**a**, **b**), 40 mm (**c**), 20 mm (**d**), 10 mm (**e**), 5 mm (**f**).

Article



Extended Data Fig. 4 | Phylogenetic position of *Helicoloceillus cantorigen*. et sp. nov. All taxa coded in the Bayesian analysis are included in this figure. Numbers are posterior probabilities for nodes.



Extended Data Fig. 5 | Additional phylogenetic topologies run as sensitivity analyses. a, Ctenophores constrained as sister-group to all other animals³⁸.

b, Relationships of Porifera classes constrained by recent molecular phylogenies¹⁰

(see Supplementary Information for further details). Numbers are posterior probabilities for nodes.

Corresponding author(s): Shuhai Xiao

Last updated by author(s): 4/24/2024

Reporting Summary

Nature Research wishes to improve the reproducibility of the work that we publish. This form provides structure for consistency and transparency in reporting. For further information on Nature Research policies, see [Authors & Referees](#) and the [Editorial Policy Checklist](#).

Please do not complete any field with "not applicable" or n/a. Refer to the help text for what text to use if an item is not relevant to your study.

For final submission: please carefully check your responses for accuracy; you will not be able to make changes later.

Statistics

For all statistical analyses, confirm that the following items are present in the figure legend, table legend, main text, or Methods section.

n/a Confirmed

- The exact sample size (n) for each experimental group/condition, given as a discrete number and unit of measurement
- A statement on whether measurements were taken from distinct samples or whether the same sample was measured repeatedly
- The statistical test(s) used AND whether they are one- or two-sided
Only common tests should be described solely by name; describe more complex techniques in the Methods section.
- A description of all covariates tested
- A description of any assumptions or corrections, such as tests of normality and adjustment for multiple comparisons
- A full description of the statistical parameters including central tendency (e.g. means) or other basic estimates (e.g. regression coefficient) AND variation (e.g. standard deviation) or associated estimates of uncertainty (e.g. confidence intervals)
- For null hypothesis testing, the test statistic (e.g. F , t , r) with confidence intervals, effect sizes, degrees of freedom and P value noted
Give P values as exact values whenever suitable.
- For Bayesian analysis, information on the choice of priors and Markov chain Monte Carlo settings
- For hierarchical and complex designs, identification of the appropriate level for tests and full reporting of outcomes
- Estimates of effect sizes (e.g. Cohen's d , Pearson's r), indicating how they were calculated

Our web collection on [statistics for biologists](#) contains articles on many of the points above.

Software and code

Policy information about [availability of computer code](#)

Data collection

ImageJ 1.52a

Data analysis

MrBayes 3.2.6, Microsoft Excel 2013, Geomagic Warp 2017, CloudCompare v.2.13, Tracer 1.7

For manuscripts utilizing custom algorithms or software that are central to the research but not yet described in published literature, software must be made available to editors/reviewers. We strongly encourage code deposition in a community repository (e.g. GitHub). See the Nature Research [guidelines for submitting code & software](#) for further information.

Data

Policy information about [availability of data](#)

All manuscripts must include a [data availability statement](#). This statement should provide the following information, where applicable:

- Accession codes, unique identifiers, or web links for publicly available datasets
- A list of figures that have associated raw data
- A description of any restrictions on data availability

Fossils illustrated in this paper are accessioned in the Nanjing Institute of Geology and Palaeontology (catalogue numbers of NIGP-176531 to NIGP-176538, NIGP-155870, NIGP-201942). Data collected or generated during this study are included in this published article and its supplementary information files. The nomenclature acts of Helicolocellus cantori gen. et sp. nov. is registered in zoobank, and the Life Science Identifier for this publication is urn:lsid:zoobank.org:pub:06F779B0-BA00-41AF-A6F7-A552BA8F6BF1.LSID.

Field-specific reporting

Please select the one below that is the best fit for your research. If you are not sure, read the appropriate sections before making your selection.

Life sciences Behavioural & social sciences Ecological, evolutionary & environmental sciences

For a reference copy of the document with all sections, see nature.com/documents/nr-reporting-summary-flat.pdf

Ecological, evolutionary & environmental sciences study design

All studies must disclose on these points even when the disclosure is negative.

Study description	Palaeontological study of early animal fossils collected from the late Ediacaran Shibantan Member of the Dengying Formation at Wuhe village in Yichang, Hubei Province, China.
Research sample	Fossil specimens were collected from the Shibantan Member of the Dengying Formation at Wuhe village (GPS coordinates 30.790920° 111.050583°), Hubei Province, China. All specimens described in this paper are reposed in Nanjing Institute of Geology and Palaeontology. Accession numbers of illustrated specimens are provided in the manuscript.
Sampling strategy	All specimens encountered in the excavation were collected and studied. A total of 7 specimens of <i>Helicolocellus</i> were collected. This sample size is deemed sufficient in paleontological investigations. No sample size calculation was performed.
Data collection	Fossil specimens were photoed using Nikon D850 camera and Zeiss Zoom. V16. Measurements were made on photographs of specimens using ImageJ. Laser scanning data were obtained using the Faro Design ScanArm, and processed using the software Geomagic Warp and CloudCompare.
Timing and spatial scale	Fossils were collected in 2019–2023 from stratigraphic horizons about 2 m above the base of the Shibantan Member at the Wuhe section (GPS coordinates 30.790920° 111.050583°) in the Yangtze Gorges area of South China.
Data exclusions	No data were excluded from analysis.
Reproducibility	To ensure reproducibility, details about fossil locality and stratigraphic horizon have been noted.
Randomization	N/A
Blinding	N/A

Did the study involve field work? Yes No

Field work, collection and transport

Field conditions	The field site is located in the subtropical zone. Climate is humid in the field season (summer time). The outcrop is well exposed. Excavation was required to remove slabs of fossil specimens.
Location	Located at Wuhe, Yichang, Hubei Province in South China (GPS coordinates 30.790920° 111.050583°).
Access and import/export	Collection of fossil specimens was carried out in a responsible manner and in compliance with the local, national and international laws. Specimens are publicly accessible in the Nanjing Institute of Geology and Palaeontology, China, with accession numbers provided in the manuscript.
Disturbance	Disturbance was minimised by carefully controlled excavation. Reclamation of excavation quarries will be carried out after the research project is completed.

Reporting for specific materials, systems and methods

We require information from authors about some types of materials, experimental systems and methods used in many studies. Here, indicate whether each material, system or method listed is relevant to your study. If you are not sure if a list item applies to your research, read the appropriate section before selecting a response.

Materials & experimental systems

n/a	Involved in the study
<input checked="" type="checkbox"/>	Antibodies
<input checked="" type="checkbox"/>	Eukaryotic cell lines
<input type="checkbox"/>	Palaeontology
<input checked="" type="checkbox"/>	Animals and other organisms
<input checked="" type="checkbox"/>	Human research participants
<input checked="" type="checkbox"/>	Clinical data

Methods

n/a	Involved in the study
<input checked="" type="checkbox"/>	ChIP-seq
<input checked="" type="checkbox"/>	Flow cytometry
<input checked="" type="checkbox"/>	MRI-based neuroimaging

Palaeontology

Specimen provenance

The Shibantan Member of the Dengying Formation at Wuhe village (GPS coordinates 30.790920° 111.050583°), Hubei Province, China.

Specimen deposition

All specimens illustrated in this paper are reposed in the Nanjing Institute of Geology and Palaeontology, China. Accession numbers of illustrated specimens are provided in the manuscript.

Dating methods

Published U-Pb dates (Extended Data Fig. 1b).

Tick this box to confirm that the raw and calibrated dates are available in the paper or in Supplementary Information.

